

90° Ferroelectric Domains in PbTiO₃: Experimental Observation and Molecular Dynamics Simulations

Kenta Aoyagi¹, Takeshi Nishimatsu², Takanori Kiguchi², Toyohiko J. Konno²,
Yoshiyuki Kawazoe², Hiroshi Funakubo³, Anil Kumar^{4,5}, and Umesh V. Waghmare⁵

¹*Department of Materials Science, Tohoku University, Sendai 980-8579, Japan*

²*Institute for Materials Research (IMR), Tohoku University, Sendai 980-8577, Japan*

³*Department of Innovative and Engineered Materials,*

Tokyo Institute of Technology, Yokohama 226-8503, Japan

⁴*Department of Physics and Astronomy, Rutgers University,*

136 Frelinghuysen Road, Piscataway, NJ 08544-8019,

⁵*Theoretical Sciences Unit, Jawaharlal Nehru Centre for Advanced
Scientific Research (JNCASR), Jakkur, Bangalore, 560 064, India*

(Dated: November 1, 2018)

We report observation of 90° ferroelectric domain structures in transmission electron microscopy (TEM) of epitaxially-grown films of PbTiO₃. Using molecular dynamics (MD) simulations based on first-principles effective Hamiltonian of bulk PbTiO₃, we corroborate the occurrence of such domains showing that it arises as metastable states only in cooling simulations (as the temperature is lowered) and establish characteristic stability of 90° domain structures in PbTiO₃. In contrast, such domains do not manifest in similar simulations of BaTiO₃. Through a detailed analysis based on energetics and comparison between PbTiO₃ and BaTiO₃, we find that 90° domain structures are energetically favorable only in the former, and the origin of their stability lies in the polarization-strain coupling. Our analysis suggests that they may form in BaTiO₃ due to special boundary condition and/or defect-related inhomogeneities.

PACS numbers: 64.60.De, 68.37.Lp, 77.80.Dj, 77.80.B-, 77.84.-s

I. INTRODUCTION

Ferroelectric transitions in perovskite oxides, such as BaTiO₃, are fluctuation driven first-order phase transitions, and hence a state with spatially fluctuating order parameter can readily form as a result of certain mechanical and electric boundary conditions¹. A common example of such a state is the one with domains of ferroelectric polarization with different symmetry equivalent orientations of order parameter that are separated by domain walls. Indeed, many properties of perovskite ferroelectrics depend on such domain structure, and it is being increasingly relevant at nano-scale²⁻⁵. Naturally, the properties of a domain wall or an interface between adjacent ferroelectric domains depend on (a) symmetries and structural details of ferroelectric phases and (b) microscopic couplings responsible for the ferroelectric phase transition.

Perovskite oxides such as BaTiO₃ and PbTiO₃ are representative ferroelectric materials, although are quite different from each other in terms of their phase transitions. While PbTiO₃ undergoes a single strongly first order phase transition from cubic to tetragonal structure as temperature is lowered, BaTiO₃ exhibits a sequence of three relatively weaker first-order phase transitions. A paraelectric phase of BaTiO₃ with cubic structure transforms into a tetragonal ferroelectric phase at a Curie temperature, 393 K. Further cooling produces sudden changes from a tetragonal phase to an orthorhombic phase at 278 K and from an orthorhombic phase to a rhombohedral phase at 203 K^{6,7}. On the other

hand, PbTiO₃ exhibits a phase transition from a paraelectric cubic phase to a ferroelectric tetragonal phase at $T_C = 763$ K and remains tetragonal down to 0 K⁸⁻¹⁰.

While the domain structures in ferroelectrics have been revealed experimentally^{7,11-25}, detailed *in situ* experimental analysis of the domains and domain walls is quite challenging and the temperature dependence of dynamics of domain structure is not well understood. In the case of PbTiO₃, experimental studies of domains are further more difficult as the sample needs to be heated over its *high* transition temperature $T_C = 763$ K and such heating leads to evaporation of Pb ions changing the composition of the sample²⁶.

Ferroelectric phase transitions in perovskite oxides in bulk and thin film have been investigated by computer simulations such as phase-field method²⁷, Monte Carlo simulations²⁸, and molecular dynamics (MD) simulations²⁹. Recently, Nishimatsu *et al.* have developed a fast and versatile MD simulator of ferroelectrics based on first-principles effective Hamiltonian³⁰ which can be used in systematic studies of bulk as well as thin films. They have studied BaTiO₃ bulk and thin-film capacitors and obtained results showing good agreement with experiments. Their MD simulations of BaTiO₃ under periodic boundary condition (PBC) for bulk did not show any domain structures, as there is no depolarization field in the PBC of bulk. Simulations of thin-film of BaTiO₃ only show 180° domain structures³⁰, though 90° domain structures are widely seen in experiments^{11,13}. One of the advantages of MD simulations compared to Monte Carlo simulations is its ability to simulate

time-dependent dynamical phenomena, e.g. MD simulation can be used to study the evolution of ferroelectric domains as a function of time during heating-up and cooling-down simulations.

In this paper, we report heating-up and cooling-down molecular-dynamics (MD) simulations of bulk PbTiO_3 to understand our observation of 90° domain structures in epitaxially-grown sample of PbTiO_3 . In Sec. II, we present experimental details for the sample preparation and we show a transmission electron microscope (TEM) image of 90° domain structure in PbTiO_3 film. We briefly explain the first-principles effective Hamiltonian and details of MD simulations in Sec. III and we present our results and analysis of heating-up and cooling-down MD simulations in Sec. IV. We finally summarize our work and conclusions in Sec. V.

II. EXPERIMENTAL DETAILS AND OBSERVATIONS

A. Sample preparation and Methods of TEM

An epitaxial PbTiO_3 thick film, with film thicknesses of about 1200 nm, was grown on the $\text{SrRuO}_3/\text{SrTiO}_3$ substrate at 873 K by pulsed metal organic chemical vapor deposition (pulsed-MOCVD) method. SrRuO_3 was deposited on (100) SrTiO_3 by rf-magnetron sputtering method. The detail of film preparation technique is described elsewhere^{31,32}. The TEM specimens were prepared with focused ion beam (FIB) micro-sampling technique. Damage layers, introduced during FIB microfabrication, were removed by low-energy Ar ion milling at 0.3 kV. JEM-2000EXII was used for TEM observations. TEM observations were performed at room temperature.

B. Observed TEM image

In Fig. 1, we show a bright field TEM image of a PbTiO_3 thick film, taken with the incident electron beam parallel to the $[100]$ axis of the PbTiO_3 . The inset in the image is the corresponding selected-area electron diffraction pattern. This bright-field TEM image is taken with the scattering vector $g_{01\bar{1}}$ excited. Here, a - and c -domains are those with polarization along a and c axes of the PbTiO_3 parallel and perpendicular to the substrate, respectively. This domain configuration is typical and very commonly seen for tetragonal PbTiO_3 films. The domain size is about 50-200 nm. Such 90° domain configurations, similar to that in Fig. 1, have been also observed in BaTiO_3 ^{11,13}. Boundaries between a - and c -domains are seen as black lines, as the TEM sample is slightly tilted. From this image, we can not discuss the width of domain walls between a - and c -domain. High-resolution TEM observation has revealed that the width of 90° domain walls is $1.0 \pm 0.3 \text{ nm}$ ³³. To this end, high-resolution TEM observation was conducted in order to reveal the

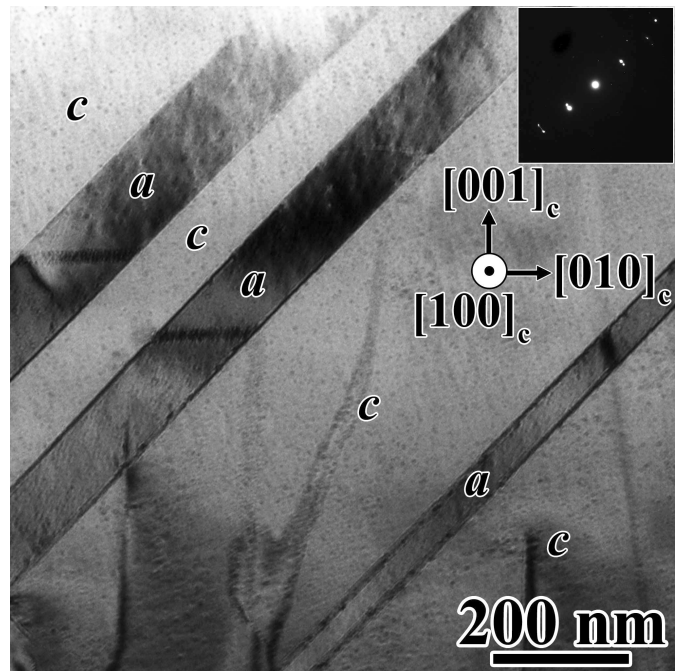


FIG. 1: A bright-field TEM image of a PbTiO_3 thick film taken with an electron incident parallel to the $[100]$ of PbTiO_3 . Scripts a and c in this figure denote a -domain and c -domain, respectively.

width of domain walls between a - and c -domain. Fig. 2 shows the high-resolution TEM image of PbTiO_3 film, indicating that the width of domain walls is corresponding to 1 or 2 unit cells.

Before our computational study, it should be worth mentioning that 90° domains have been often observed in both BaTiO_3 and PbTiO_3 , and are both ferroelectric and ferroelastic in nature. Typically, 90° domains are formed in epitaxial ferroelectric and ferroelastic films in order to relax the strain resulting from lattice mismatch with the substrate at and below T_C ^{34,35}. They nucleate at misfit dislocations formed above T_C . Their growth is accompanied with the introduction of the additional dislocation perpendicular to the misfit dislocations and the dissociation of the dislocations into two pairs of partial dislocations around an anti-phase boundary²³.

III. MOLECULAR DYNAMICS SIMULATIONS

A. Effective Hamiltonian

Heating-up and cooling-down molecular-dynamics (MD) simulations are performed using first-principles effective Hamiltonian^{28-30,36,37},



FIG. 2: A high-resolution TEM image of a PbTiO₃ thick film taken with an electron incident parallel to the [100] of PbTiO₃. The 90° domain boundary is shown by the chain line.

$$\begin{aligned}
H^{\text{eff}} = & \frac{M_{\text{dipole}}^*}{2} \sum_{\mathbf{R}, \alpha} \dot{u}_{\alpha}^2(\mathbf{R}) + \frac{M_{\text{acoustic}}^*}{2} \sum_{\mathbf{R}, \alpha} \dot{w}_{\alpha}^2(\mathbf{R}) \\
& + V^{\text{self}}(\{\mathbf{u}\}) + V^{\text{dpl}}(\{\mathbf{u}\}) + V^{\text{short}}(\{\mathbf{u}\}) \\
& + V^{\text{elas, homo}}(\eta_1, \dots, \eta_6) + V^{\text{elas, inho}}(\{\mathbf{w}\}) \\
& + V^{\text{coup, homo}}(\{\mathbf{u}\}, \eta_1, \dots, \eta_6) + V^{\text{coup, inho}}(\{\mathbf{u}\}, \{\mathbf{w}\}), \quad (1)
\end{aligned}$$

where $\mathbf{u} = \mathbf{u}(\mathbf{R})$ and $\mathbf{w} = \mathbf{w}(\mathbf{R})$ are, respectively, the local dipolar displacement vector and the local acoustic displacement vector of the unit cell at \mathbf{R} in a simulation supercell. $\alpha (= x, y, z)$ is the Cartesian directions. Braces $\{\}$ denote a set of \mathbf{u} or \mathbf{w} in the supercell. η_1, \dots, η_6 are the homogeneous strain components. M_{dipole}^* and M_{acoustic}^* are the effective masses for \mathbf{u} and \mathbf{w} , therefore, first two terms in Eq. (1) are kinetic energies of them.

V^{self} , V^{dpl} , V^{short} , $V^{\text{elas, homo}}$, $V^{\text{elas, inho}}$, $V^{\text{coup, homo}}$, and $V^{\text{coup, inho}}$ are a local-mode self-energy, a long-range dipole-dipole interaction, a short-range interaction, a homogeneous elastic energy, an inhomogeneous elastic energy, a coupling between $\{\mathbf{u}\}$ and η_1, \dots, η_6 , and a coupling between $\{\mathbf{u}\}$ and $\{\mathbf{w}\}$, respectively. More detailed explanation of symbols in the effective Hamiltonian can be found in Refs. 30 and 37. We take all the parameters of the first-principles effective Hamiltonian for PbTiO₃ from the earlier work³⁸. However, the form of the effective Hamiltonian we use in our simulations^{30,37} is slightly different from the one used to get the parameters in Ref. 38.

TABLE I: The parameters of first-principles effective Hamiltonian for PbTiO₃ used in our simulations are given in the second column and how these parameters are related with the parameters in the previous work³⁸ are shown in the third column.

parameters	value	relation
a_0 [Å]	3.969	a_0
B_{11} [eV]	117.9	C_{11}
B_{12} [eV]	51.6	C_{12}
B_{44} [eV]	137.0	C_{44}
B_{1xx} [eV/Å ²]	-114.02	$2(g_0 + g_0)$
B_{1yy} [eV/Å ²]	-13.67	$2g_0$
B_{4yz} [eV/Å ²]	-22.67	g_2
α [eV/Å ⁴]	27.83	$B + C$
γ [eV/Å ⁴]	-34.48	$-2C$
k_1 [eV/Å ⁶]	-42.42	D
k_2 [eV/Å ⁶]	0	
k_3 [eV/Å ⁶]	0	
k_4 [eV/Å ⁸]	156.43	E
m^* [amu]	100.0	
Z^* [e]	10.02	Z^*
ϵ_{∞}	8.24	ϵ_{∞}
κ_2 [eV/Å ²]	1.170	A
j_1 [eV/Å ²]	-1.355	$2a_T$
j_2 [eV/Å ²]	4.986	$2a_L$
j_3 [eV/Å ²]	0.222	$b_l + b_{t1}$
j_4 [eV/Å ²]	-0.018	$2b_{t2}$
j_5 [eV/Å ²]	0.398	$b_l - b_{t1}$
j_6 [eV/Å ²]	-0.083	$\frac{2(c_l + 2c_t)}{3}$
j_7 [eV/Å ²]	-0.204	$\frac{2(c_l - 2c_t)}{3}$

The new parameters can be easily derived from the previous ones. We list values of all the parameters used in our simulations and how they are related to the previous work³⁸ in Table I.

B. Simulation Details

Heating-up and cooling-down MD simulations are performed with our original MD code `feram` (<http://loto.sourceforge.net/feram/>). Details of the code can be found in Ref. 30. Temperature is kept constant in each temperature step in the canonical ensemble using the Nosé-Poincaré thermostat.³⁹ This symplectic thermostat is so efficient that we can set the time step to $\Delta t = 2$ fs. In our present MD simulations, we thermalize the system for 20,000 time steps, after which we average the properties for 20,000 time steps. We used a supercell of system size $N = L_x \times L_y \times L_z = 32 \times 32 \times 32$ and small temperature steps in heating-up (+1 K/step) and cooling-down (-1 K/step) simulations. The heating-up simulation from 100 K to 900 K is started from an z -polarized initial

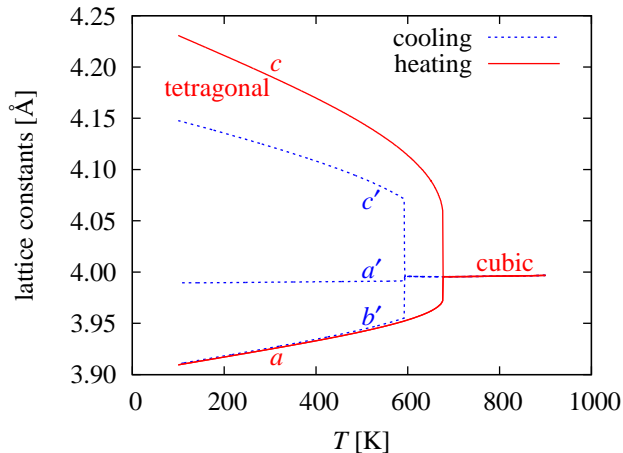


FIG. 3: (Color online) Simulated temperature dependence of lattice constants of PbTiO_3 in heating-up (red solid lines) and cooling-down (blue dashed lines) molecular-dynamics simulations.

configuration generated randomly: $\langle u_x \rangle = \langle u_y \rangle = 0$, $\langle u_z \rangle = 0.33 \text{ \AA}$, $\langle u_x^2 \rangle - \langle u_x \rangle^2 = \langle u_y^2 \rangle - \langle u_y \rangle^2 = (0.045 \text{ \AA})^2$, and $\langle u_z^2 \rangle - \langle u_z \rangle^2 = (0.021 \text{ \AA})^2$, where brackets denote \mathbf{R} -average in supercell $\langle u_\alpha \rangle = \frac{1}{N} \sum_{\mathbf{R}} u_\alpha(\mathbf{R})$. The cooling-down one from 900 K to 100 K is started from random paraelectric initial configuration: $\langle u_x \rangle = \langle u_y \rangle = \langle u_z \rangle = 0$ and $\langle u_\alpha^2 \rangle - \langle u_\alpha \rangle^2 = (0.15 \text{ \AA})^2$.

IV. RESULTS AND DISCUSSION

From the temperature dependence of averaged lattice constants (shown in Fig. 3), a tetragonal-to-cubic ferroelectric-to-paraelectric phase transition is clearly observed in the heating-up simulation at 677 K. However, a strange behavior in lattice constants is found in the cooling-down simulation at $T=592 \text{ K}$. The average temperature of these two transition temperatures (634 K) is in good agreement with the earlier Monte Carlo simulations and slightly lower than the experimental value $T_C = 763 \text{ K}$. Indeed, the observation of an orthorhombic phase during cooling-down simulations is intriguing.

To understand this interesting behaviour of lattice constants in cooling-down simulations, we perform a detailed analysis of the configurations (snapshots) during our MD simulations. From a snapshot of dipoles in the supercell (shown in Fig. 4), we find that the apparently orthorhombic nature of the phase is due to a 90° domain structure. Although the 4 unit cell = 1.6 nm of the domain size is much smaller than experimentally observed ones as shown in Sec. II B, the width of a simulated domain wall estimated to be ~ 1 unit cell is in good agreement with our experiment. Each domain has the $a = b < c$ tetragonal structure of PbTiO_3 , but their average value in whole crystal gives smaller c' than c and larger a' than a . The lattice constant b' has almost the same values as

a , because the polar directions of two kind of domains are perpendicular to the b' -axis. It should be noted that this domain structure is found in MD simulations in bulk under periodic boundary condition (PBC), but we have not simulated thin films. Under the PBC, there is no depolarization field inside the bulk. Moreover, this domain structure can be easily reproduced in cooling-down simulations from any random paraelectric initial configurations and any seeds for the pseudo random number generator⁴⁰. There was no evidence for such unusual behavior in simulations of bulk BaTiO_3 ^{30,37}.

To understand the reason of stability of the 90° domain structure seen here, even in bulk PbTiO_3 , we compare “total energy surfaces” between single and 90° domain structures. The total energy surface of single domain structure with $[001]$ polarization is the same as in Refs. 36 and 30. For the total energy surface of 90° domain structure, we focus on a snapshot of the supercell at 300K shown in Fig. 4 and represent it with $\{\mathbf{u}_{90^\circ,300\text{K}}(\mathbf{R})\}$. We now obtain a sequence of configurations by multiplying a factor $\frac{u}{\langle u \rangle_{90^\circ,300\text{K}}}$ for all \mathbf{R}

$$\mathbf{u}(\mathbf{R}) = \frac{u}{\langle u \rangle_{90^\circ,300\text{K}}} \mathbf{u}_{90^\circ,300\text{K}}(\mathbf{R}), \quad (2)$$

and compute total energy as a function of u , where $\langle u \rangle_{90^\circ,300\text{K}}$ is the averaged length of dipoles in the 300 K snapshot

$$\langle u \rangle_{90^\circ,300\text{K}} = \frac{1}{N} \sum_{\mathbf{R}} |\mathbf{u}_{90^\circ,300\text{K}}(\mathbf{R})| = 0.32 \text{ \AA}. \quad (3)$$

Calculated total energy surfaces of single and 90° domain structures for PbTiO_3 are shown in Fig. 5 with solid and dashed lines, respectively. For comparison, those for BaTiO_3 are also plotted assuming the same 90° domain structure by using the set of parameters in H^{eff} listed in Ref. 37. While the 90° domain structure of PbTiO_3 exhibits a minimum at $u \neq 0$, that of BaTiO_3 costs energy. This is why the 90° domain structures can be found in simple cooling-down simulations of PbTiO_3 , but not in those of BaTiO_3 .

Minima are indicated with (a)–(c) in Fig. 5. To uncover the origin of this contrasting behaviour, interaction energy terms at the minimums are listed in TABLE II. For the BaTiO_3 , because there is no minimum, interaction energies of configuration at (d) in Fig. 5 (of $u = 0.10 \text{ \AA}$) are listed.

From TABLE II, It is clear that the energy losses in V^{harmonic} , $V^{\text{elas, inho}}$, and $V^{\text{coup, homo}}$ in forming the 90° domain structure in PbTiO_3 are compensated by the energy gains in $V^{\text{unharmonic}}$, $V^{\text{elas, homo}}$, and $V^{\text{coup, inho}}$. In contrast, such recovery is not sufficient in BaTiO_3 to form a $u \neq 0$ minimum or non trivial 90° domain structures. In stabilization of the 90° domain structures in PbTiO_3 , our analysis conclusively highlights the role of two microscopic interactions: (a) lower elastic energy cost arising from the smaller strain from compensation along c

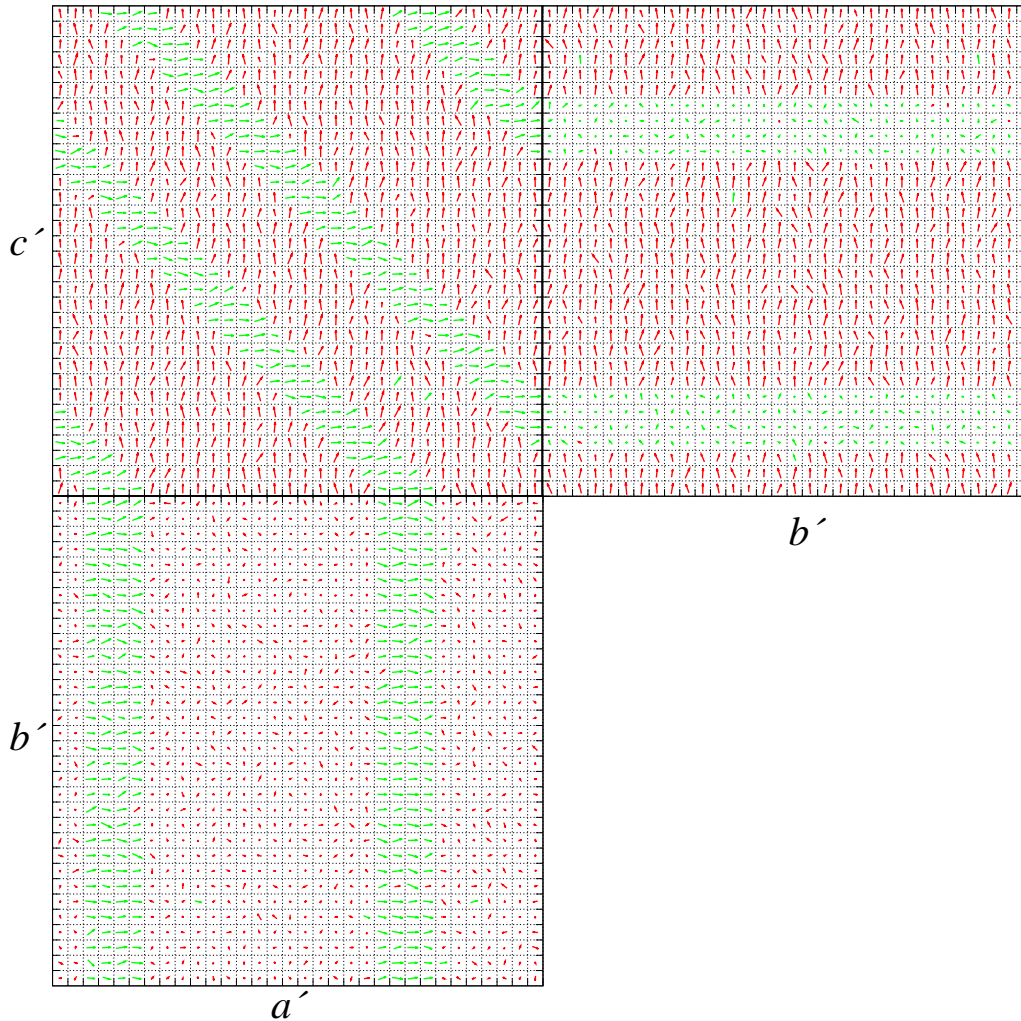


FIG. 4: (Color online) Snapshot of three “sides” of the $32 \times 32 \times 32$ supercell at $T = 300\text{K}$ in a cooling-down simulation of PbTiO_3 . Dipole moments of each site are projected onto the side planes and indicated with arrows. Dipoles of $u_z > 0.2\text{\AA}$ are indicated with red color. Dipoles of $u_z \leq 0.2\text{\AA}$ are indicated with green. Crystalline directions are indicated with a' , b' , and c' as indicated in Fig. 3.

TABLE II: Comparison of interaction energies V^i in the effective Hamiltonian of Eq. (1) for two kinds of domain states of PbTiO_3 and BaTiO_3 . V^{harmonic} is the sum of V^{dpl} , V^{short} , and the harmonic terms in V^{self} . $V^{\text{unharmonic}}$ is the unharmonic terms in V^{self} . Unit of energy is eV.

x of interaction energy V^x	PbTiO_3 (a) single domain	PbTiO_3 (b) 90° domain	ΔV^i	BaTiO_3 (c) single domain	BaTiO_3 (d) 90° domain	ΔV^i
harmonic	-0.22106	-0.14393	+0.07713	-0.03886	0.03541	+0.07427
unharmonic	0.33435	0.17249	-0.16186	0.04754	0.00695	-0.04059
elas,homo	0.21946	0.04441	-0.17505	0.02609	0.00131	-0.02478
elas,inho	0.00000	0.05171	+0.05171	0.00000	-0.00262	-0.00262
coup,homo	-0.43891	-0.08881	+0.35010	-0.05218	0.00089	+0.05307
coup,inho	0.00000	-0.10342	-0.10342	0.00000	-0.00178	-0.00178
total	-0.10616	-0.06755	+0.03861	-0.01741	0.04016	+0.05757
u [\AA]	0.34	0.29		0.16	0.10	

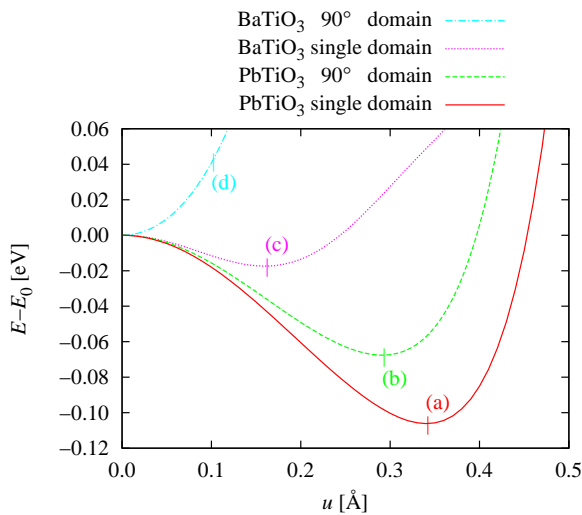


FIG. 5: (Color online) Calculated total energy surfaces for PbTiO₃ single domain (solid line), PbTiO₃ 90° domain (dashed line), BaTiO₃ single domain (dotted line), and BaTiO₃ 90° domain (chain line).

and a axis, and (b) inhomogeneous (local) strain coupling with polarization at the domain wall. The latter does not contribute much to transition behavior in the bulk, but has rather significant impact on the properties of domain wall. Noting that a 90° domain structure is not energetically favorable in BaTiO₃ simulated as a perfect bulk crystal and coupling of soft modes with higher energy modes is weak, we believe that the experimentally observed 90° domain structures in BaTiO₃ is most likely due to inhomogeneities in the samples and/or the specific electric and mechanical boundary conditions.

V. SUMMARY

In this article, TEM observation of PbTiO₃ thick films revealed 90° domain structures, which have been often observed in BaTiO₃. The domain size perpendicular to domain boundaries was 50–200 nm. The width of domain wall was corresponding to 1 or 2 unit cell.

We also have performed heating-up and cooling-down MD simulations of PbTiO₃. In cooling-down simulation, 90° domain structure is found to form spontaneously. By comparing “total energy surfaces” of single and 90° domain structures, we understand that a 90° domain structure is metastable in bulk PbTiO₃, but not in bulk BaTiO₃. The origin of this contrast is traced to significantly larger polarization-strain coupling in PbTiO₃. Hence, while 90° domain structures can form spontaneously in PbTiO₃, they seem to arise in BaTiO₃ mostly from special boundary conditions and/or defect-related inhomogeneities.

Acknowledgments

This work was supported by Japan Society for the Promotion of Science (JSPS) through KAKENHI 23740230 and 21760524. Computational resources were provided by the Center for Computational Materials Science, Institute for Materials Research (CCMS-IMR), Tohoku University. We thank the staff at CCMS-IMR for their constant effort. This study was also supported by the Next Generation Super Computing Project, Nanoscience Program, MEXT, Japan. UVW acknowledges an IBM faculty award grant in supporting some of his work.

-
- ¹ A. Kumar and U. V. Waghmare, Phys. Rev. B **82**, 054117 (2010).
 - ² A. Schilling, D. Byrne, G. Catalan, K. G. Webber, Y. A. Genenko, G. S. Wu, J. F. Scott, and J. M. Gregg, Nano Letters **9**, 3359 (2009), pMID: 19591494.
 - ³ I. A. Luk'yanchuk, A. Schilling, J. M. Gregg, G. Catalan, and J. F. Scott, Phys. Rev. B **79**, 144111 (2009).
 - ⁴ D. D. Fong, G. B. Stephenson, S. K. Streiffer, J. A. Eastman, O. Auciello, P. H. Fuoss, and C. Thompson, Science **304**, 1650 (2004).
 - ⁵ J. Paul, T. Nishimatsu, Y. Kawazoe, and U. V. Waghmare, Phys. Rev. Lett. **99**, 077601 (2007).
 - ⁶ G. Shirane and A. Takeda, J. Phys. Soc. Jpn. **6**, 128 (1951).
 - ⁷ A. von Hippel, Rev. Mod. Phys. **22**, 221 (1950).
 - ⁸ G. Shirane, S. Hoshino, and K. Suzuki, Phys. Rev. **80**, 1105 (1950).
 - ⁹ G. Shirane, R. Pepinsky, and B. Frazer, Acta Crystallogr. **9**, 131 (1956).
 - ¹⁰ G. Shirane, R. Pepinsky, and B. Frazer, Phys. Rev. **97**, 1179 (1955).
 - ¹¹ A. Schilling, T. B. Adams, R. M. Bowman, J. M. Gregg, G. Catalan, and J. F. Scott, Phys. Rev. B **74**, 024115 (2006).
 - ¹² B. J. Rodriguez, L. M. Eng, and A. Gruverman, Appl. Phys. Lett. **97**, 042902 (2010).
 - ¹³ T. Matsumoto, M. Koguchi, K. Suzuki, H. Nishimura, Y. Motoyoshi, and N. Wada, Appl. Phys. Lett. **92**, 072902 (2008).
 - ¹⁴ I. A. Luk'yanchuk, A. Schilling, J. M. Gregg, G. Catalan, and J. F. Scott, Phys. Rev. B **79**, 144111 (2009).
 - ¹⁵ J. Fousek and M. Safranko, Jpn. J. Appl. Phys. **4**, 403 (1965).
 - ¹⁶ M. Tanaka and G. Honjo, J. Phys. Soc. Jpn. **19**, 954 (1964).
 - ¹⁷ M. Tanaka, N. Kitamura, and G. Honjo, J. Phys. Soc. Jpn. **17**, 1197 (1962).
 - ¹⁸ T. Matsumoto and M. Okamoto, J. Appl. Phys. **109**, 014104 (2011).
 - ¹⁹ H. Nakaki, Y. K. Kim, S. Yokoyama, R. Ikariyama, H. Funakubo, S. K. Streiffer, K. Nishida, K. Saito, and A. Gruverman, J. Appl. Phys. **104**, 064121 (2008).
 - ²⁰ H. Nakaki, Y. K. Kim, S. Yokoyama, R. Ikariyama, H. Funakubo, K. Nishida, and K. Saito, Appl. Phys. Lett. **91**, 112904 (2007).
 - ²¹ K. Lee and S. Baik, Ann. Rev. Mater. Res. **36**, 81 (2006).

- ²² K. Aoyagi, T. Kiguchi, Y. Ehara, T. Yamada, H. Funakubo, and T. J. Konno, *Sci. Technol. Adv. Mater.* **12**, 034403 (2011).
- ²³ T. Kiguchi, K. Aoyagi, Y. Ehara, H. Funakubo, T. Yamada, N. Usami, and T. J. Konno, *Sci. Technol. Adv. Mater.* **12**, 034413 (2011).
- ²⁴ S. Stemmer, S. Streiffer, F. Ernst, M. Rühle, W. Hsu, and R. Raj, *Solid State Ion.* **75**, 43 (1995).
- ²⁵ W. Hsu and R. Raj, *Appl. Phys. Lett.* **67**, 792 (1995).
- ²⁶ R. Gerson, *J. Appl. Phys.* **31**, 188 (1960).
- ²⁷ Y. L. Li, S. Y. Hu, Z. K. Liu, and L. Q. Chen, *Applied Physics Letters* **78**, 3878 (2001).
- ²⁸ W. Zhong, D. Vanderbilt, and K. M. Rabe, *Phys. Rev. B* **52**, 6301 (1995).
- ²⁹ U. V. Waghmare, E. J. Cockayne, and B. P. Burton, *Ferroelectrics* **291**, 187 (2003).
- ³⁰ T. Nishimatsu, U. V. Waghmare, Y. Kawazoe, and D. Vanderbilt, *Phys. Rev. B* **78**, 104104 (2008).
- ³¹ K. Nagashima and H. Funakubo, *Jpn. J. Appl. Phys.* **39**, 212 (2000).
- ³² K. Nagashima, M. Aratani, and H. Funakubo, *Jpn. J. Appl. Phys.* **39**, L996 (2000).
- ³³ S. Stemmer, S. K. Streiffer, F. Ernst, and M. Rühle, *Phil. Mag. A* **71**, 713 (1995).
- ³⁴ W. Pompe, X. Gong, Z. Suo, and J. S. Speck, *Journal of Applied Physics* **74**, 6012 (1993).
- ³⁵ J. S. Speck and W. Pompe, *J. Appl. Phys.* **76**, 466 (1994).
- ³⁶ R. D. King-Smith and D. Vanderbilt, *Phys. Rev. B* **49**, 5828 (1994).
- ³⁷ T. Nishimatsu, M. Iwamoto, Y. Kawazoe, and U. V. Waghmare, *Phys. Rev. B* **82**, 134106 (2010).
- ³⁸ U. V. Waghmare and K. M. Rabe, *Phys. Rev. B* **55**, 6161 (1997).
- ³⁹ S. D. Bond, B. J. Leimkuhler, and B. B. Laird, *J. Comput. Phys.* **151**, 114 (1999).
- ⁴⁰ G. Marsaglia and W. W. Tsang, *Statistics & Probability Letters* **66**, 183 (2004).